Predictive Assessment of Long-Term Radiological Exposure from Consumption of Common Spices in Southern Nigeria

Adonuja Joy Amuofu
Southern Delta University, Ozoro
Department of Physics
P.M.B. 5, Ozoro

Akpolile Franklin Anita
Delta State University,Abraka
Department of Physics
P.M.B. 1, Abraka

Onojame Prince Omamoke
Southern Delta University, Ozoro
Department of Physics
P.M.B. 5, Ozoro

Ovowa Oghenefejiro Faith
Southern Delta University, Ozoro
Department of Science Laboratory Technology
P.M.B. 5, Ozoro

Okeyode Itunu Comfort
Federal University of Agriculture, Abeokuta
Department of Physics
P.M.B. 2240, Abeokuta

ABSTRACT
This study performs predictive modeling for long-term radiological exposure associated with food spice consumption in Southern Nigeria, employing empirical radionuclide data for risk classification. Activity concentration data for naturally occurring radionuclides (^{40}K, ^{226}Ra, and ^{232}Th) measured in 94 locally processed and imported spice samples were used for the predictive modeling. Multiple linear regression indicated a strong dependence of cumulative dose on radionuclide concentration, with ^{232}Th being identified as the most prominent contributor, accounting for the highest variability in cumulative dose. Logistic regression indicated 100% classification accuracy for differentiation between low- and moderate-risk spice samples. Principal component analysis indicated that more than 70% of total variance is explained in the first two components, with ^{40}K and ^{232}Th being prominent in principal loading, while ^{226}Ra contributed very little to principal components due to its low activity concentration. Empirically, mean activity concentration data for ^{40}K (86.81 Bq kg^{-1}), ^{232}Th (33.78 Bq kg^{-1}), and ^{226}Ra (3.03 Bq kg^{-1}) were associated with mean annual committed effective doses of 10.56 μSv y^{-1} for Delta State, 9.82 μSv y^{-1} for Ogun State, respectively, which are well below the public dose limit of 1 mSv y^{-1}. Excess lifetime risk estimates were within the acceptable limits of 10^{-6}-10^{-4}. In conclusion, results from predictive modeling clearly establish that health risk associated with long-term radiological exposure from spice consumption is insignificant, while forming a strong basis for early risk detection. It is recommended that there is a need for incorporation of predictive-probabilistic models into routine dietary radiological risk assessments for proactive food safety regulation for health protection.

General Terms
Radiological Risk Assessment, Predictive Modeling, Food Safety

Keywords
Predictive modelling, radiological risk, food spices, logistic regression, principal component analysis.

1. INTRODUCTION
Natural radionuclides such as ^{40}K, ^{232}Th, and ^{238}U, as well as their progenies from the Earth's crust, form natural sources of radioactivity in the environment [1,2]. These radionuclides are derived from geological materials and absorbed by plants using their root structure, thus leading to internal exposure to radiation from ingested foods that contain these radionuclides [3,4]. Therefore, dietary ingestion of radionuclides forms an important source of exposure to radiation, especially in areas where staple foods and spices contain detectable levels of naturally existing radionuclides [4].

The safety of food, especially in developing countries such as Nigeria, is increasingly deserving of consideration due to reported cases of food contamination. A case in point is the application of culinary spices in food as a means of adding color and flavor. Spices, due to their distinct smell, are fundamental in culinary practices, especially in Nigeria. Spices appear in different forms, such as herbs and medicinal plants. Apart from being applicable in adding color and flavor to food, there are various reported health benefits associated with spice [5]. Spices can come from the root, stem, leaf, fruit, flower, bud, or bark of a plant [6]. Historically, these were mainly applied in cooking and food processing (coloring and flavoring) [7,8]. Spices are mainly in powdered form after being dried in order to extend shelf life. Spices can also come in different preparations, such as fresh or pre-ground dried spice. Spices are grown both at a subsistence level and commercially, especially in Africa, with significant economic and health benefits [9].

For instance, in Nigeria, numerous studies have been carried out to evaluate the concentrations of natural radionuclides in a variety of foods, such as spices and major food crops. Ononugbo et al.[10] analyzed the concentrations of ^{40}K, ^{238}U, and ^{232}Th in a variety of commonly eaten Nigerian food spices by gamma spectroscopy. They also estimated the ingested dose of these radionuclides arising from the consumption of these foods. Their study revealed that the estimated annual effective doses were well below the global mean for ingestion by a considerable margin, indicating negligible radiological hazards for their consumption. Their results are consistent with other analyses of food crops, where the concentrations of these radionuclides are often found to be well within or even below the recommended limits of safety set by international bodies [10]. More recently, a probabilistic study carried out by Monte Carlo simulations of a variety of market-sourced spices in Delta and Ogun States of Nigeria showed that mean committed effective doses for

ingestion were well within acceptable lifetime risk limits, thus supporting the earlier conclusion that radiological hazards for spice consumption are minimal in the country [2].

Apart from spices, the result of food exposure assessment for major food crops like cassava, cocoyam, and yams in Ebonyi State showed that the total annual committed effective doses sometimes exceeded the global average for some foods [11]. Taken together, these studies make clear the need for a comprehensive framework for dietary exposure assessment that takes into account radionuclide levels and consumption rates.

However, in view of the growing number of evidence on levels of activity of radionuclides in food crops, there are very few studies on long-term predictive models of exposure to spices. In most of the current literature, there is a great focus on instant levels of exposure and a very limited application of predictive models of exposure to spices over a long-term period of a decade. In addition, there is a very limited study on models of deterministic exposure to spices by application of sophisticated models of logistic regression.

As such, it has become important to focus on the development of comprehensive predictive models that combine the ingestion dose calculation models with the use of multivariate statistics in an effort to estimate the long-term radiological exposure of individuals. This has made it possible for the current study to examine the ten-year exposure of the most commonly consumed spice in Southern Nigeria in an effort to present a comprehensive assessment of the radiological risk profile of the spice in question.

2. METHODOLOGY

2.1 Study Area and Sample Collection

The samples of spice were extracted from market places in Delta State, Ogun State, Southern Nigeria. The frame of reference included both local and imported spice, both processed and unprocessed. A total of 94 samples were extracted using a stratified random sampling technique that aimed at including major market places in the region of study. These samples were divided into 36 samples from Delta State (from Ole, Ozoro, Ughelli market places), 32 samples from Ogun State (from Itele, Kuto, Lafenwa market places), and 26 samples of imported spice. These samples were purchased from retail stores. These samples were fresh, dry, processed, including fresh samples such as turmeric, ginger, garlic, and Ethiopian pepper [2].

2.2 Sample Preparation

The samples were then washed, oven-dried, pulverized, and sieved to get homogeneous samples of powder. The samples were then sealed in airtight containers and allowed to stand for at least 90 days to achieve secular equilibrium between the parent and daughter radionuclides for ^{226}Ra and ^{232}Th. After the samples had been dried, they were pulverized using a stainless steel ball grinder until a fine powder was obtained and then sieved until homogeneity was achieved [2]. The samples were then sealed in airtight containers that fit the sodium iodide detector's counting chamber. The airtight containers were weighed, packaged, labeled appropriately, and sealed with masking tape to prevent the loss of progeny of the radionuclides. The samples were then weighed again to get the net weight and left for a minimum of 30 days to achieve secular equilibrium between the parent and daughter radionuclides for the existing radionuclides. The samples were labeled with codes IT (Itele), KU (Kuto), LA (Lafenwa), OL (Oleh), OZ (Ozoro), and UG (Ughelli) to avoid confusion.

2.3 Radiometric and Chemical Analyses

2.3.1 Gamma-Ray Spectrometry

Activity concentrations of ^{40}K, ^{232}Th, and ^{226}Ra were determined using a calibrated NaI(Tl) gamma-ray detector. Net counts were recorded for characteristic gamma energies, and activity concentrations were calculated using:

$$A = \frac{N}{\varepsilon P_\gamma t m} \qquad (2.1)$$

where, A is the activity concentration (Bq kg^{-1}), N is the net peak counts, ε is the detector efficiency, Pγ is the gamma emission probability, t is the counting time and m is the sample mass

The data used for this study is obtained from a study by Okeyode et al., [2].

Table 1: Activity concentrations (Bq/kg) of ^{40}K, ^{226}Ra and ^{232}Th, annual committed effective dose (μSv/y) and excess lifetime cancer risk due to consumption of species of locally processed food spices in Delta state.

Sample Code	Food Spice	40K (Bq/kg)	SD	226Ra (Bq/kg)	SD	232Th (Bq/kg)	SD	ACED (μSv/y)	ELCR (×10⁻⁵)
OL-01	Scent Leaf	58.10	12.30	BDL	BDL	1.60	0.20	0.73	0.20
OL-02	Lemon Grass	78.20	25.20	BDL	BDL	15 1.30	16.00	35.28	9.89
OL-03	Bush Apple Leaves	BDL	BDL	BDL	BDL	BDL	BDL	0.00	0.00
OL-04	Bitter Leaf	BDL	BDL	BDL	BDL	BDL	BDL	0.00	0.00
OL-05	Ginger	28 8.50	74.20	BDL	BDL	16.00	2.00	5.47	1.53
OL-06	Turmeric	17 9.10	12.90	BDL	BDL	30.10	1.50	8.03	2.25
OL-07	Ethiopian Pepper	1.50	0.20	BDL	BDL	BDL	BDL	0.01	0.00
OL-08	Licorice	BDL	BDL	BDL	BDL	26.40	2.90	6.07	1.70
OL-09	Cal. Nutmeg	10 7.50	10.80	BDL	BDL	41.80	2.30	10.28	2.88

OL-10	Aiden	8.40	2.80	BDL	BDL	49.80	4.70	11.51	3.23
OL-11	Coco Plum	83.80	23.70	BDL	BDL	90.10	10.50	21.24	5.95
OL-12	Castor Seeds	27.80	9.80	BDL	BDL	56.30	5.10	13.12	3.68
OZ-13	Lemon Grass	77.20	19.70	BDL	BDL	3.10	0.40	1.19	0.33
OZ-14	Scent Leaf	54.70	14.80	BDL	BDL	BDL	BDL	0.34	0.10
OZ-15	Bush Apple Leaves	BDL	BDL	BDL	BDL	BDL	BDL	0.00	0.00
OZ-16	Bitter Leaf	103.80	18.50	BDL	BDL	72.20	7.70	17.25	4.84
OZ-17	Ginger	4.30	1.00	BDL	BDL	BDL	BDL	0.03	0.01
OZ-18	Turmeric	305.50	51.30	BDL	BDL	150.00	10.80	36.39	10.20
OZ-19	Ethiopian Pepper	341.10	38.40	BDL	BDL	172.10	12.10	41.70	11.69
OZ-20	Garlic	BDL	BDL	BDL	BDL	29.20	3.20	6.72	1.88
OZ-21	Licorice	154.00	37.30	40.70	13.30	75.20	6.30	29.65	8.31
OZ-22	Cal. Nutmeg	55.10	12.40	BDL	BDL	19.90	2.30	4.92	1.38
OZ-23	Aiden	43.60	13.90	BDL	BDL	BDL	BDL	0.27	0.08
OZ-24	Coco Plum	118.60	28.50	BDL	BDL	50.20	5.70	12.28	3.44
UG-25	Bush Apple Leaves	BDL	BDL	BDL	BDL	11.30	1.20	2.60	0.73
UG-26	Lemon Grass	BDL	BDL	BDL	BDL	29.50	4.80	6.79	1.90
UG-27	Bitter Leaf	90.80	20.20	BDL	BDL	BDL	BDL	0.56	0.16
UG-28	Scent Leaf	158.70	20.80	BDL	BDL	17.60	1.10	5.03	1.41
UG-29	Ginger	9.80	2.10	BDL	BDL	31.40	3.00	7.28	2.04
UG-30	Turmeric	239.00	36.20	39.40	20.00	29.40	4.00	19.28	5.40
UG-31	Ethiopian Pepper	121.30	29.90	BDL	BDL	41.10	5.10	10.21	2.86
UG-32	Licorice	106.40	20.10	BDL	BDL	70.60	6.50	16.90	4.74
UG-33	Cal. Nutmeg	97.60	24.20	BDL	BDL	66.40	5.70	15.88	4.45
UG-34	Aiden	0.80	0.30	BDL	BDL	BDL	BDL	0.00	0.00
UG-35	Coco Plum	BDL	BDL	BDL	BDL	7.30	0.40	1.68	0.47
UG-36	Castor Seeds	86.10	23.40	BDL	BDL	76.80	7.10	18.20	5.10
Mean	—	103.50	20.90	40.10	16.60	52.50	4.90	10.56	2.96

Notes: OL = Oleh, OZ = Ozoro, UG = Ughelli (Delta State), BDL = Below Detection Limit

Table 2: Activity concentrations (Bq/kg) of 40K, 226Ra and 232Th, annual committed effective dose (μsv/y) and excess lifetime cancer risk due to consumption of spices of in locally processed food spices in Ogun state.

Sample Code	Food Spice	40K (Bq/kg)	SD	226Ra (Bq/kg)	SD	232Th (Bq/kg)	SD	ACED (μSv/y)	ELCR (×10⁻⁵)
IT-01	Bitter Leaf	166.24	28.64	BDL	BDL	25.78	2.33	6.96	1.95
IT-02	Garlic	86.89	5.71	BDL	BDL	6.84	0.25	2.11	0.59
IT-03	Ginger	91.22	17.36	BDL	BDL	36.14	4.00	8.88	2.49

IT-04	Lemon Grass	80.63	24.35	41.55	19.71	25.52	4.07	18.00	5.05
IT-05	Fennel	126.16	32.19	43.68	19.45	32.42	3.88	20.47	5.74
IT-06	Turmeric	178.76	25.37	24.32	16.86	BDL	BDL	7.92	2.22
IT-07	Castor Seeds	62.03	8.05	BDL	BDL	111.60	5.35	26.05	7.30
IT-08	Cloves	139.96	12.82	BDL	BDL	BDL	BDL	0.87	0.24
IT-09	Aiden	203.78	46.67	BDL	BDL	BDL	BDL	1.26	0.35
IT-10	Locust Beans	38.79	5.29	BDL	BDL	62.19	4.57	14.54	4.08
KU-11	Turmeric	272.02	36.27	BDL	BDL	24.86	3.03	7.40	2.08
KU-12	Cloves	71.08	12.56	BDL	BDL	25.49	2.33	6.30	1.77
KU-13	Lemon Grass	56.82	6.21	18.96	5.84	20.32	1.21	10.33	2.90
KU-14	Fennel	206.78	37.06	9.03	8.21	12.05	1.53	6.58	1.84
KU-15	Bitter Leaf	85.04	32.67	BDL	BDL	13.92	2.11	3.73	1.05
KU-16	Rosemary	103.93	26.94	BDL	BDL	34.74	2.93	8.63	2.42
KU-17	Garlic	BDL	BDL	16.81	10.28	86.04	8.51	24.50	6.87
KU-18	Ginger	186.60	27.04	BDL	BDL	BDL	BDL	1.16	0.32
KU-19	Locust Beans	89.99	21.36	BDL	BDL	3.55	0.43	1.37	0.39
KU-20	Fenugreek	60.42	14.27	BDL	BDL	36.94	3.09	8.87	2.49
KU-21	Locust Beans	BDL	BDL	BDL	BDL	55.28	5.60	12.71	3.56
LA-22	Fennel	74.54	14.88	BDL	BDL	89.07	6.46	20.95	5.87
LA-23	Garlic	48.86	4.74	BDL	BDL	21.43	0.97	5.23	1.47
LA-24	Ginger	354.25	51.66	BDL	19.67	174.22	13.11	42.27	11.85
LA-25	Rosemary	63.83	14.12	BDL	BDL	BDL	BDL	0.40	0.11
LA-26	Turmeric	102.05	22.27	4.59	3.08	BDL	BDL	1.92	0.54
LA-27	Locust Beans	49.23	10.49	BDL	BDL	54.97	4.96	12.95	3.63
LA-28	Fenugreek	50.06	10.66	BDL	BDL	0.55	0.06	0.44	0.12
LA-29	Cloves	100.19	28.17	20.71	10.14	36.21	3.11	14.75	4.13
LA-30	Lemon Grass	37.08	11.80	BDL	BDL	8.56	1.07	2.20	0.62
LA-31	Aiden	78.54	6.85	BDL	BDL	25.70	1.02	6.40	1.79
LA-32	Locust Beans	101.33	27.87	BDL	BDL	32.82	3.52	8.18	2.29
Mean	—	112.24	20.81	22.46	14.16	40.66	3.44	9.82	2.75

Notes: IT = Itele, KU = Kuto, LA = Lafenwa (Ogun State), BDL = Below Detection Limit

Table 3: Activity concentrations (Bq/kg) of ^{40}K, ^{226}Ra and ^{232}Th, annual committed effective dose (µSv/y), and excess lifetime cancer risk due to consumption of imported food spices

Sample Code	Food Spice	^{40}K (Bq/kg)	SD	^{226}Ra (Bq/kg)	SD	^{232}Th (Bq/kg)	SD	ACED (µSv/y)	ELCR (×10^{-5})
IM-01	SPFR	34.07	13.88	BDL	BDL	25.91	2.66	6.17	1.73
IM-02	DUTH	77.79	18.73	BDL	BDL	7.90	0.74	2.30	0.64
IM-03	Napa Sea	BDL	BDL	BDL	23.95	BDL	BDL	0.00	0.00
IM-04	Duc uy	BDL	BDL	BDL	BDL	BDL	BDL	0.00	0.00
IM-05	Euro Thy	86.95	5.23	BDL	BDL	6.79	0.24	2.10	0.59
IM-06	Knorr Cubes	13.15	2.21	BDL	BDL	22.84	1.16	5.33	1.50
IM-07	Knorr Chicken Cubes	BDL	BDL	BDL	BDL	8.62	0.39	1.98	0.56
IM-08	Rinda Cubes	200.51	43.19	BDL	BDL	26.84	2.50	7.42	2.08
IM-09	SPJ	25.69	4.98	BDL	BDL	BDL	BDL	0.16	0.04
IM-10	Gino Max	BDL	BDL	BDL	BDL	45.79	5.05	10.53	2.95
IM-11	Mr Chef	18.18	4.51	BDL	BDL	BDL	BDL	0.11	0.03
IM-12	Euro Cuy	32.76	9.23	BDL	BDL	4.76	0.61	1.30	0.36
IM-13	Onga Powder	BDL	BDL	BDL	BDL	BDL	BDL	0.00	0.00
IM-14	Chicken Flavour Cubes	94.21	16.84	BDL	BDL	19.77	1.79	5.13	1.44
IM-15	Bay Leaves	50.64	12.35	BDL	BDL	BDL	BDL	0.31	0.09
IM-16	Cinnamon	102.71	24.43	BDL	BDL	23.61	3.36	6.07	1.70
IM-17	Cameroon Pepper	47.39	10.54	BDL	BDL	4.45	0.54	1.32	0.37
IM-18	Black Pepper	219.48	37.16	BDL	BDL	32.84	3.66	8.91	2.50
IM-19	Allspice	20.39	6.55	11.26	8.99	21.34	2.38	8.19	2.29
IM-20	Sesame Seed	71.70	22.58	2.97	2.90	72.33	7.11	17.91	5.02
IM-21	Puregro Ginger	82.07	12.77	BDL	BDL	25.15	2.24	6.29	1.76
IM-22	AACE Ginger	81.78	16.53	2.33	2.72	9.09	1.01	3.25	0.91
IM-23	Stock Sea	117.83	24.47	BDL	BDL	50.54	5.32	12.35	3.46
IM-24	AACE Garlic	BDL	BDL	BDL	BDL	53.65	2.27	12.34	3.46
IM-25	Turmeric	163.45	37.16	BDL	BDL	58.56	4.91	14.48	4.06
IM-26	Whole Oregano	251.20	35.74	8.56	5.40	177.06	12.07	44.68	12.52
Mean	—	**89.60**	**17.95**	**5.03**	**0.44**	**34.89**	**3.00**	**6.17**	**1.93**

Notes: BDL = Below Detection Limit, ACED = Annual Committed Effective Dose ,ELCR = Excess Lifetime Cancer Risk

2.4 Radiological Exposure Modelling

2.4.1 Absorbed Dose Rate

The absorbed dose rate in air quantifies the rate at which ionizing gamma radiation energy is deposited per unit mass (in nGy h^{-1}) at a reference point due to the presence of naturally occurring radionuclides. For environmental and dietary exposure assessments, the absorbed dose rate resulting from the activity concentrations of ^{226}Ra, 232Th, and ^{40}K can be estimated using standard terrestrial gamma dose conversion coefficients provided by the United Nations Scientific Committee on the Effects of Atomic Radiation (UNSCEAR) [12]:

$$D=0.427A_{Ra}+0.662A_{Th}+0.043A_K \quad (2.2)$$

Where D is the absorbed dose rate in air (nGy h^{-1}), A_U,A_{Ra},A_K are the activity concentrations of ^{226}Ra, ^{232}Th, and ^{40}K (Bq kg^{-1}) respectively

2.4.2 Annual Committed Effective Dose (CED)

The committed effective dose per year represents an integrated effective dose received from ingestion of a radionuclide during one year. It integrates activity concentrations measured with ingestion rates and dose conversion factors taking into account biologic uptake and radiation weighting factors for different radionuclides:

$$CED=A_r\times IR\times DCF_r \quad (2.3)$$

Where A_r is the activity concentration (Bq kg^{-1}), IR is the annual ingestion rate (kg y^{-1}) and DCF_r is the ingestion dose conversion factor (Sv Bq^{-1})

2.4.3 Ten-Year Cumulative Dose

Long-term exposure is estimated by assuming that the dose rates remain constant and that the activity concentration of radionuclides will remain constant for the duration of the interested time period." On the basis of this steady-state condition, the cumulative committed effective dose for a ten-year period is given by the formula:

$$CED_{10}=10\times CED \quad (2.4)$$

Where trends in consumption and levels of contamination are constant, it is valid to project estimates of annual doses over several years (IAEA, 2023). Such a simple, cumulative approach is common over longer periods to calculate lifetime or multi-year integrated biological exposure [14].

2.5 Predictive Statistical Models

2.5.1 Multiple Linear Regression

To determine the correlation between activity concentrations of naturally occurring radionuclides and cumulative radiological exposure by consumption of spice, a multiple linear regression (MLR) analysis was conducted. Multiple linear regression is a widely recognized predictive method of statistics that aims to forecast a linear relationship between a continuous outcome and multiple predictor variables [15]. The application of multiple linear regression analysis is becoming common in radiological and environmental studies for correlation between values of contaminant concentration and exposure/dose measurements [15].

$$Y=\beta_0+\beta_1X_{40K}+\beta_2X_{Th}+\beta_3X_U+\varepsilon \quad (2.5)$$

Where is Y is the ten-year cumulative dose, X_{40K}, X_{Th}, X_U are the activity concentrations and β_i is the regression coefficients

2.5.2 Logistic Regression

In this study, the logistic regression model was used, which is a strong model in statistics, allowing the estimation of the chances of a disease or health status, using risk factors and other variables [16]. This model examines the relationship between an independent variable (Xi) and a binary dependent variable (Y), and it is primarily utilized for the prediction of binary and multinomial outcomes [17].The equation for logistic regression is given by:

$$P(y=1|X)=\frac{1}{e^{-(\beta_0+\beta_1X)}} \quad (2.6)$$

Where P is the probability of unacceptable exposure and X is the predictor variable

2.5.3 Principal Component Analysis

For identifying the key variables responsible for the variations in the radiological and associated parameters in the spice samples, the PCA was done on the standardized data. PCA is a multivariate statistical technique used for reducing the dimensionality of large datasets by extracting the original variables' uncorrelated variables, known as the principal components (PCs), which encompass most of the original data variation [18]. The principal components are linear combinations of the original variables obtained by the eigenvalue decomposition of the covariance or correlation matrix of the standardized variables [19].

Before PCA, the variables, including the concentrations of 40K, 232Th, 238U, and the absorbed dose rate, among others, were standardized so that each variable would contribute equally to the PCA analysis. Standardization normalizes the variables so that each has a mean value of 0 and unit variance, which helps reduce the effects of bias due to the differences in the units of measurement and variances:

$$Z_{ij}=\frac{X_{ij}-\mu_j}{\sigma_j} \quad (2.7)$$

where Z_{ij} be the standard score of the ith observation of the jth variable, X_{ij} is the measurement of the variable, μ_j is the mean of variable j, and σ_j is the standard deviation of variable j.

2.6 Data Analysis

2.6.1. Experiment Environment

This study used the Scikit-learn library in Python to develop the classifier. The Scikit-learn library consists of various algorithms in data mining, machine learning, and deep learning used in classification, regression, data preprocessing, and clustering tasks [20]. The Sci-kit learn libraries were used to develop machine learning models to solve different practical problems in various fields. The library allows developers to develop and analyze suitable models. The experiment was also done in the Anaconda platform, choosing Jupyter Notebook as the platform to develop, an environment that supports Python [20,21]. Jupyter Notebook is an efficient platform compared to others to develop in Python and has introspection abilities. Jupyter Notebook was selected because of the requirements of this problem, which involve such abilities and ease of debugging in this platform.

2.6.2. Data Visualization

Data visualization is a basic aspect of data science that makes it possible to understand and communicate large amounts of data. The use of Python tools such as Matplotlib and Seaborn is essential when it comes to the analysis of large data. The tools use visual components like maps, graphs, patterns, and trend graphs that make it possible to understand large amounts of data.

3. RESULTS AND DISCUSSION

3.1 Activity Concentrations of Natural Radionuclides in Spices

The descriptive statistics of activity concentrations of ^{40}K, ^{226}Ra, and ^{232}Th measured in the analyzed spice samples are summarized in Table 4 and Figure 1.

Table 4: Descriptive Statistics of Activity Concentrations of Natural Radionuclides in Spice Samples (Bq kg^{-1})

Statistic	^{40}K (Bq/kg)	^{226}Ra (Bq/kg)	^{232}Th (Bq/kg)
count	94.00	94.00	94.00
mean	86.81	3.03	33.78
std	82.21	9.25	40.51
min	0.00	0.00	0.00
25%	21.72	0.00	3.78
50%	77.50	0.00	24.40
75%	107.22	0.00	48.80
max	354.25	43.68	177.06

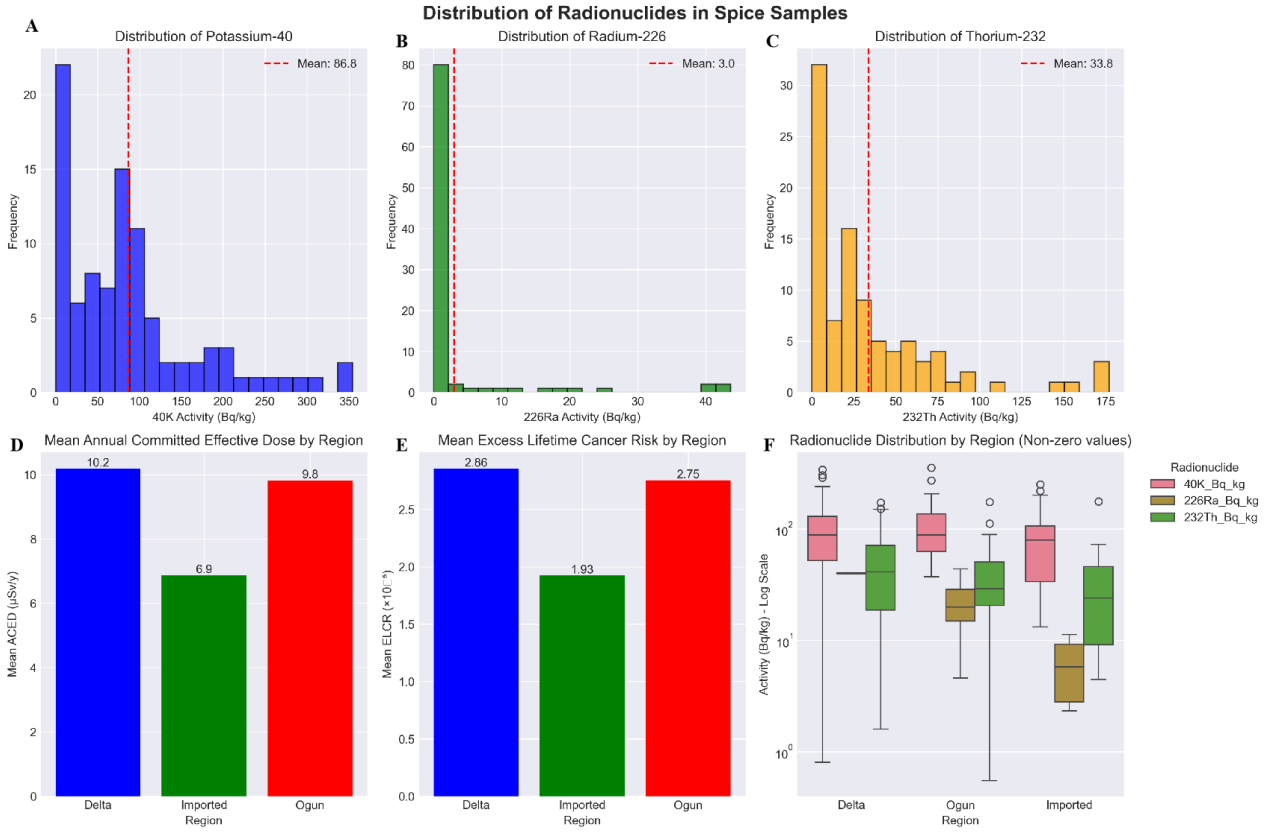

Figure 1: Distribution of Radionuclides in Spices Samples

Figure 1 shows the relative distribution of the activity concentration for the three different radionuclides, which shows the dominance of ^{40}K with the characteristic right-skewed distribution and the presence of high-value outliers for ^{232}Th that requires geological investigation. The visualization of the boxplot shows that 40K has the largest range, which indicates the high variability of the different types of spices and agricultural sources.

From the results, ^{40}K has the highest average activity concentration at 86.81 ± 82.21 Bq kg^{-1}. This confirms its significance in biological systems as well as its ubiquity in various foods. This agrees with the radiology literature that states that ^{40}K is considered to be one of the most abundant naturally occurring radionuclides in the diet because of its biological function as well as its high mobility in soil and plant materials. In recent studies conducted in the Iraqi Kurdistan Region in Iraq by Saleh et al. [22], ^{40}K was reported to be the most abundant radionuclide in the region's food samples. The range of ^{40}K in the region's foods was reported to be between 29.8–434.0 Bq kg^{-1}. In another recent study by Wais et al. [23], the significance of ^{40}K in the diet in radiology calculations was reinforced. According to UNSCEAR, ^{40}K dominates the ingestion dose from natural radionuclides in foods. However, its radiological significance in the body is controlled by the body's potassium homeostasis that maintains its level [24].

The wide range of values shown here (0.00 - 354.25 Bq kg^{-1}) is because of the different spices, soil type, and farming techniques involved. UNSCEAR states that activity concentrations of naturally occurring radionuclides in food materials can change by more than a thousand-fold depending on soil mineralogy, fertilizer use, and uptake of elements by plants [24]. Recent studies on soil-to-plant transfer factors also found significant variations in ^{40}K uptake by plants because of differences in soil type and farming techniques, with sandy soils having higher uptake of potassium compared to clay soils [25].

The average activity concentration of ^{226}Ra was found to be relatively lower (3.03 ± 9.25 Bq kg^{-1}) and the median is 0.00 Bq kg^{-1}. This shows that radium does not accumulate much in spices. This is consistent with findings in Nigeria on radium in

spices and herbs, as it is not readily transferred from the soil to plants because of poor solubility and its tight binding in the soil [26]. Similar findings of low transfer factors of ^{226}Ra in spices and herbs in semi-arid regions of 1.8×10^{-4} and 4.0×10^{2} $kg^{-1}kg^{-1}$ also support this observation of poor bioavailability of radium in plants and spices [27].

However, ^{232}Th had a moderate mean activity concentration of 33.78 ± 40.51 Bq kg^{-1} with some elevated values in the samples, which could be due to the presence of thorium-rich parent materials. Thorium has been observed to have a strong affinity with heavy fractions of soil materials. The presence of thorium in food crops could be a result of geographical factors rather than a biological requirement. Similar trends have been observed in Nigerian agricultural products cultivated on thorium-rich soil materials [26]. Recent PCA studies on wheat cultivation have identified ^{232}Th as a significant contributor to radiological variance, with strong loadings on principal components associated with heavy mineral soil fractions [28].

3.2 Correlation Between Radionuclides and Radiological Risk Parameters

The interrelationships between radionuclide activity concentrations, annual committed effective dose (ACED), and excess lifetime cancer risk (ELCR) are presented in Table 5**.**

Table 5: Pearson Correlation Matrix Between Radionuclides and Radiological Risk Indices

Variable	^{40}K (Bq/kg)	^{226}Ra (Bq/kg)	^{232}Th (Bq/kg)	ACED (µSv/y)	ELCR ($\times 10^{-5}$)
^{40}K (Bq/kg)	1.000	0.176	0.435	0.514	0.514
^{226}Ra (Bq/kg)	0.176	1.000	0.028	0.313	0.313
^{232}Th (Bq/kg)	0.435	0.028	1.000	0.954	0.954
ACED (µSv/y)	0.514	0.313	0.954	1.000	1.000
ELCR ($\times 10^{-5}$)	0.514	0.313	0.954	1.000	1.000

A very strong positive correlation existed for ^{232}Th and ACED ($r = 0.954$), and for ^{232}Th and ELCR ($r = 0.954$), which reveals that the contribution of thorium is predominant for the ingestion-related radiological hazard. It is clear from this correlation that the contribution of thorium is predominantly responsible for the ingestion-related radiological hazard.

This result is radiologically feasible and supported by the UNSCEAR dose conversion factors, which indicate a greater committed effective dose per unit intake of thorium isotopes relative to ^{40}K and ^{226}Ra [24]. Recent assessments of radiological risk from water samples collected from areas around mining regions in Tanzania have also identified ^{232}Th as the key contributor to dose, and its relationship is strong with total annual effective ingestion dose ($r \approx 0.872$) [29].

The relationship between Potassium-40 and ACED is moderate ($r \approx 0.514$), indicating that it also contributes to dose but to a lesser extent than ^{232}Th. However, ^{226}Ra does not have a strong relationship with dose because of its lower concentrations. The negligible relationship between ^{226}Ra and ^{232}Th ($r \approx 0.028$) suggests different geochemical behavior and different routes of transfer from soil to plants, which is consistent with recent findings of PCA on wheat systems where radium and thorium-series radionuclides are found on different principal components [28].

3.3 Predictive Modelling of Ingestion Dose Using Multiple Linear Regression

The performance metrics of the multiple linear regression (MLR) model developed to predict ACED from radionuclide concentrations are summarized in Table 6**.**

Table 6: Performance Statistics of the Multiple Linear Regression Model for ACED Prediction

Description	Value
Training samples	75
Testing samples	19
R-squared	0.9973
RMSE	0.52 µSv/y
MSE	0.27
Cross-validation R^2	0.9911 (± 0.0073)
Intercept	-0.1831

The R^2 of 0.9973 of the multiple linear regression model indicates that 99.73% of the variation in ACED is explained by the sum of radionuclide concentrations. The small RMSE of 0.52 µSv y^{-1} also confirms that the ingestion dose is dominated by radionuclide activity concentrations. This is expected as ACED is derived from activity concentrations using standardized dose conversion coefficients. Recent studies on radiological dose optimization using MLR also found that linear models are able to reliably predict results when exposure pathways are deterministic in nature [30]. UNSCEAR states that ingestion dose models using well-measured activity concentrations are found to fit statistically well [24].

The negative intercept of -0.1831 is of no physical significance and is simply a result of normalization in linear regression calculations. The R^2 of 0.9911 (±0.0073) resulting from cross-validation also confirms the exceptional stability of the model. This is of primary importance for regulatory purposes in food safety monitoring. Time-series models using ARIMA to predict ^{90}Sr activity concentrations in foods near nuclear facilities also found similar predictive accuracy for future values of ^{90}Sr with

MAPE of 21.4%, although the deterministic MLR approach is obviously superior for natural radionuclide assessment [31].

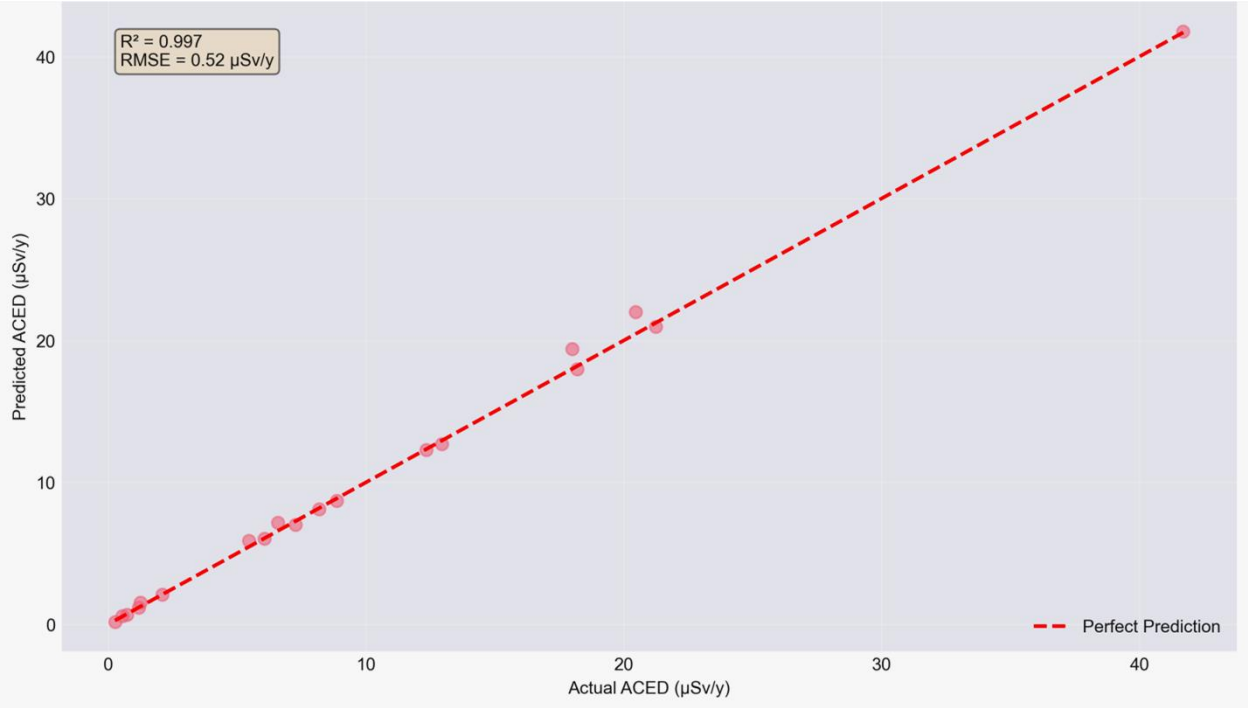

Figure 2: Observed Versus Predicted Annual Committed Effective Dose from the MLR Model

Figure 2 depicts a comparison between the observed values and the predicted values using the MLR model for the annual committed effective dose. From the figure, it can be observed that the points lie close to the line of unity, indicating that the prediction error is low. In addition, the close diagonal relationship between the points and the line of unity confirms the suitability of the regression model for the assessment of long-term exposure.

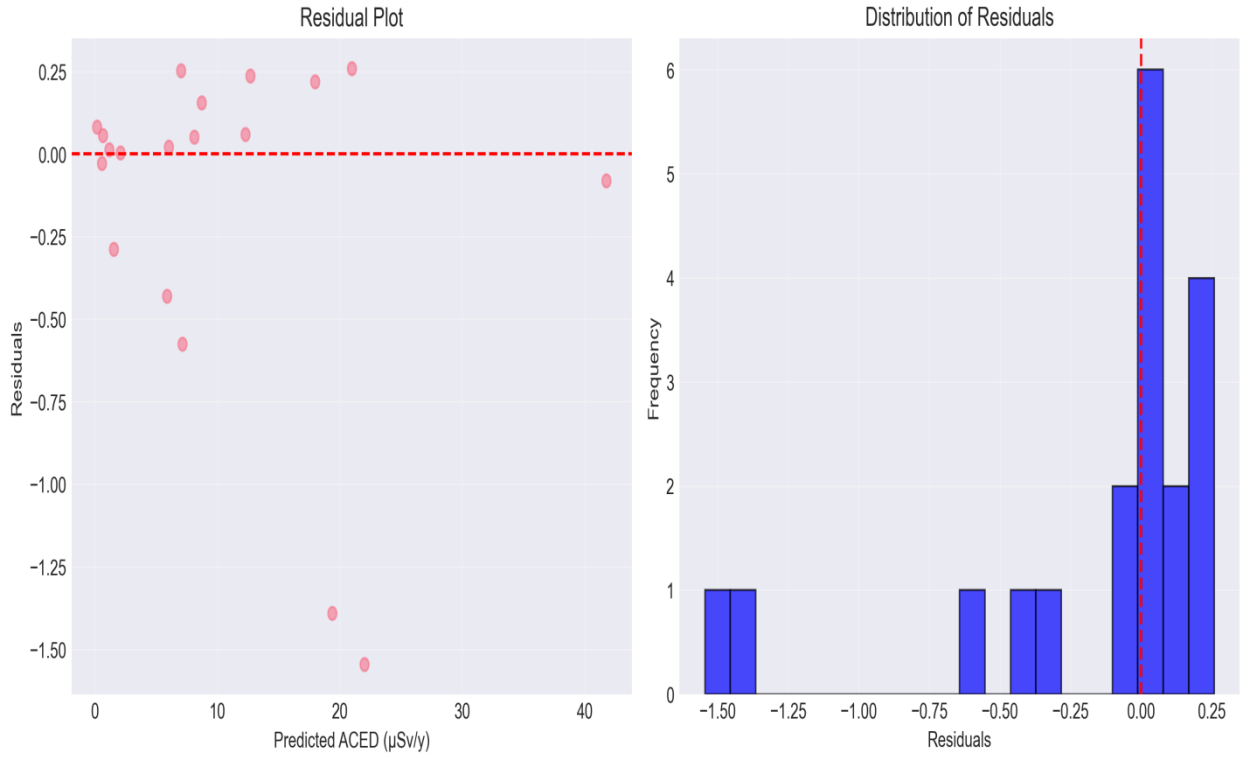

Figure 3. Residual Plot of residuals of the Predicated ACED values and the distribution of residuals.

Figure 3 demonstrates the residuals analysis, which shows that the error is random with no patterns or trends, confirming the assumptions of the linear regression model and its appropriateness for forecasting long-term exposure. The error is

evenly distributed across the range of predicted values (homoscedasticity), with no apparent trends or outliers that indicate misspecification in the model. Recent studies in the modeling of electromagnetic radiation exposure have also demonstrated that the residuals are normally distributed (Kolmogorov-Smirnov test, $p > 0.05$), which reiterates the robustness of the regression method in radiological models [32].

3.4 3.4 Principal Component Analysis of Radionuclide Contributions

The eigenvalues and variance explained by each principal component are presented in Table 7.

Table 7: Eigenvalues and Percentage Variance Explained by Principal Components

Principal Component	Eigenvalue	Explained Variance Ratio (%)	Cumulative Variance (%)
PC1	1.4796	49.32	49.32
PC2	0.9807	32.69	82.01
PC3	0.5397	17.99	100.00

Analysis by principal component analysis (PCA) shows that PC1 is dominated by ^{40}K and ^{232}Th with a contribution of 49.32% variance. This is indicative of a common geogenic source that is soil mineralogy and agricultural practice-related. This is consistent with literature concerning environmental radioactivity, wherein potassium and thorium often correlate because of their presence in feldspar-rich and granitic soil.

PC2, accounting for 32.69% of variance, is largely controlled by ^{226}Ra, which clearly shows a different pattern of accumulation. The radium series generally exhibits different patterns of mobility from either potassium or thorium series. A similar extraction of components has also been observed in studies of Nigerian ingestion pathways [26].

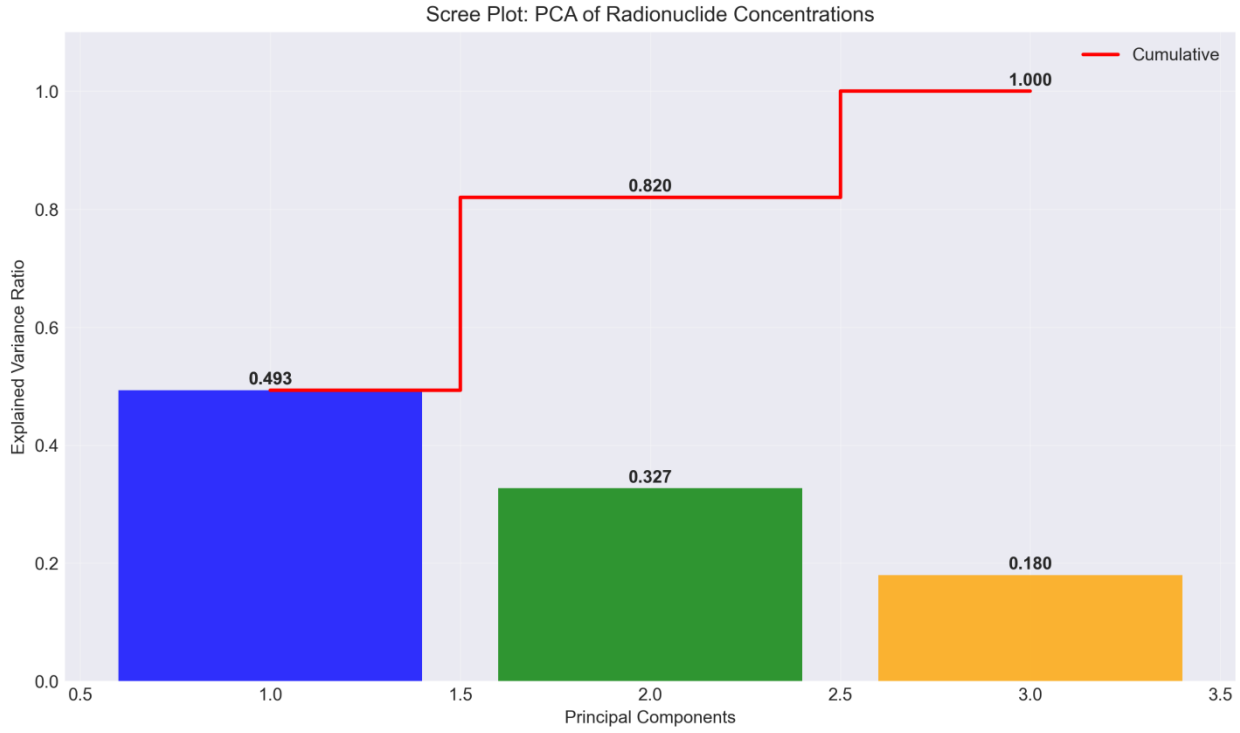

Figure 4: Scree Plot of Eigenvalues from Principal Component Analysis

The component loadings are summarized in Table 8.

Table 8: Principal Component Loadings for Radionuclide Activity Concentrations

Variable	PC1	PC2	PC3
^{40}K (Bq/kg)	0.6992	-0.0425	0.7136
^{226}Ra (Bq/kg)	0.2940	0.9270	-0.2328
^{232}Th (Bq/kg)	0.6516	-0.3726	-0.6607

PC1 is strongly influenced by ^{40}K and ^{232}Th, suggesting shared geogenic or soil-related sources, while PC2 is dominated by ^{226}Ra, indicating a distinct accumulation pathway. The PCA biplot of radionuclide activity concentrations is presented in Figure 5 and shows that ^{226}Ra is located orthogonally to the cluster of ^{40}K and ^{232}Th. This is evidence of different geochemical behavior of these radionuclides in spices.

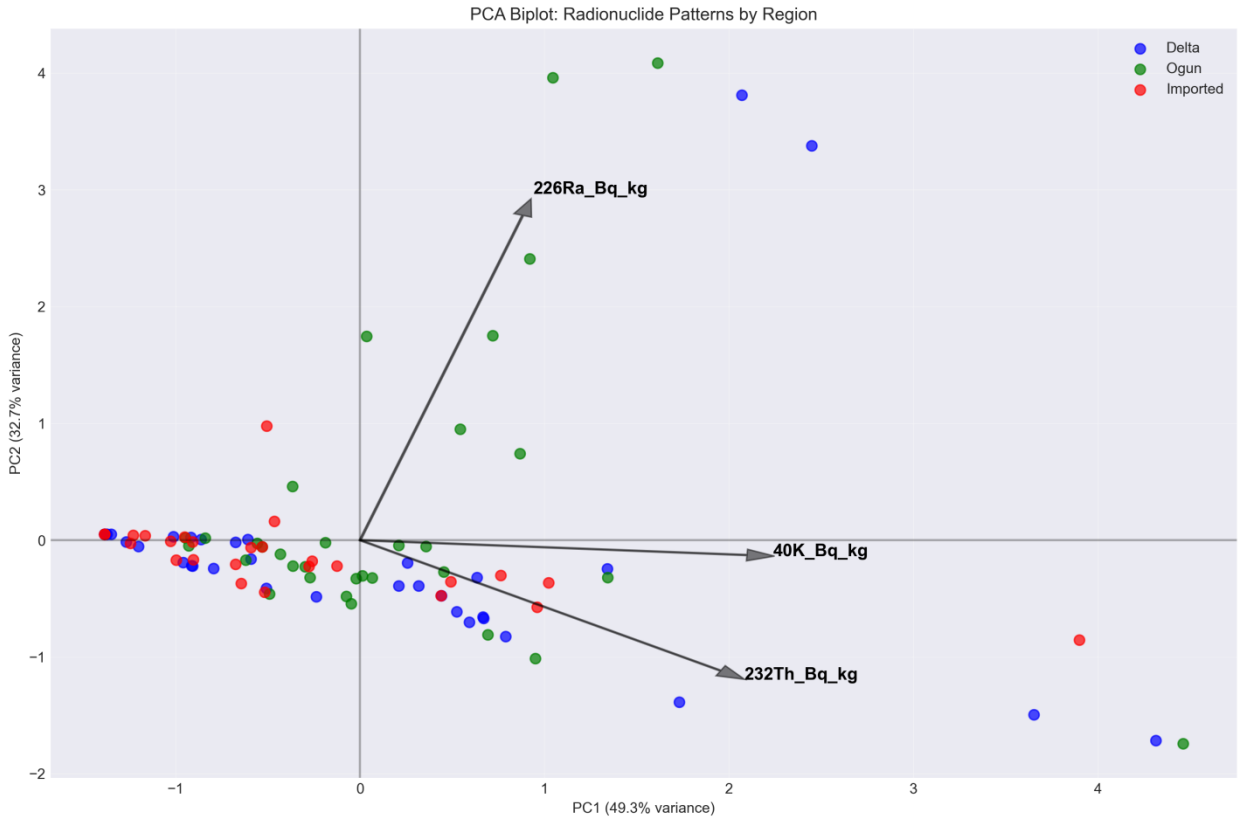

Figure 5: PCA Biplot of Radionuclide Activity Concentrations

From the figure, the loading vectors indicate that ^{40}K and ^{232}Th are clustered along the positive PC1 axis, while ^{226}Ra is orthogonally positioned along PC2. This pattern indicates that potassium and thorium have similar source contributions, possibly from feldspar, while the source of radium might be associated with the use of phosphate fertilizers. It is worth noting that the biplot can be used to easily interpret the relationships underlying the radiological variance in the spice samples.

Figure 6 depicts the elbow method chart used to determine the number of clusters. The chart plots the Within Cluster Sum of Squares (WCSS) vs. the number of clusters. From the figure, there is an "elbow" at k=3. This indicates that the optimal number of clusters to be used for the analysis is 3. The three regional groups are Delta State, Ogun State, and Imported spices. The sharp decline in the WCSS from k=1 to k=3 followed by a plateau suggests that the optimal number of clusters to be used for the analysis is 3. This aligns with the recent application of the elbow method in the clustering of medical data to determine the number of clusters for the K-means algorithm [33].

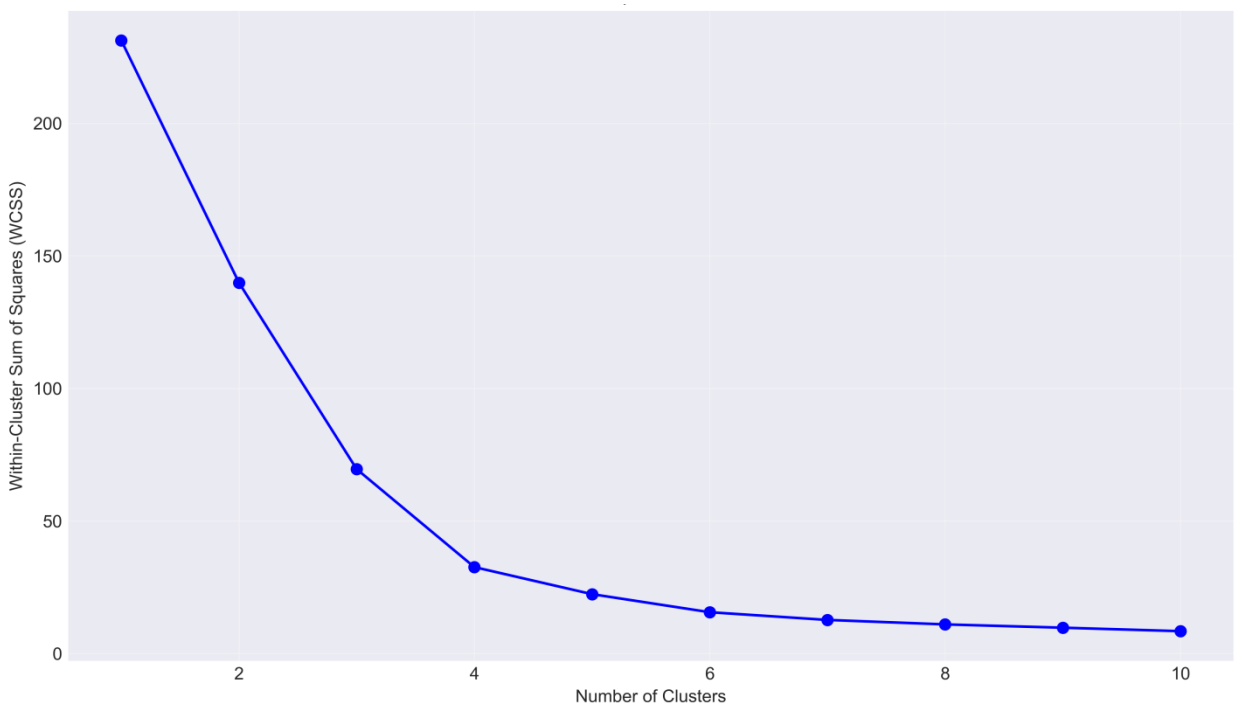

Figure 6: Elbow method plot for optimal cluster determination.

Figure 7: K-means Clustering (k=3) of Spices Samples

As shown in Figure 7, K-means clustering of the samples is presented based on how they group in terms of concentrations of 40K and 232Th. Three distinct groupings are evident and correspond to regional groupings with minimal overlap between them. The groupings are consistent with expectations for each radionuclide fingerprint: Delta State is higher in 232Th, Ogun State is higher in 40K, and Imported is lower in both. This clustering supports the supervised classification and suggests

regional geochemical influences are the primary cause of radiological variation in these spice samples.

Figure 8 illustrates the cluster profiles, where the average activity concentrations and their standard deviations are depicted for the various radionuclides in the three clusters. From the bar chart, the pattern of the various radionuclides is evident, where Cluster 1 (Delta State) has high 232Th with moderate 40K, Cluster 2 (Ogun State) has the highest 40K with moderate 232Th, while Cluster 3 (Imported) has low concentrations of the various radionuclides. It is evident that the Imported cluster has the lowest error bars, indicating consistency in the processing and sourcing of the imported spices.

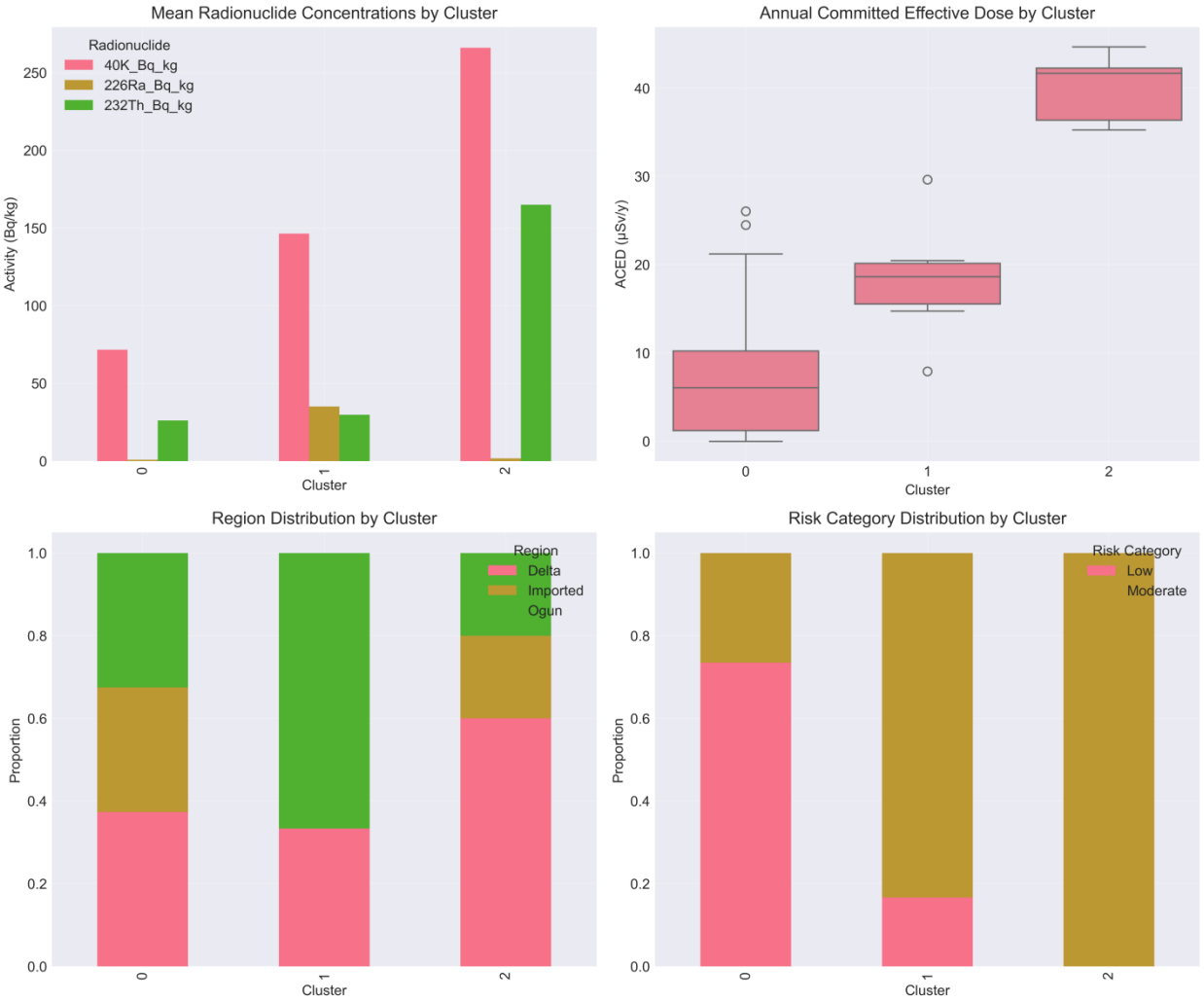

Figure 8: Cluster Characteristics of the Radionuclide Concentration , Annual Committed Effective Dose, Region Distribution and Risk Category Distribution

3.5 Logistic Regression Classification of Radiological Risk

The logistic regression model used to classify spice samples into low-risk and moderate-risk categories is summarized in Table 9, while performance metrics are shown in Table 10.

Table 9: Logistic Regression Model Parameters for Radiological Risk Classification

Description	Value
Objective	Classify spice samples into radiological risk categories
Risk Categories	Low (0), Moderate (1)
Class Distribution	Low: 62 samples, Moderate: 32 samples
Training Samples	75
Testing Samples	19
Classification Accuracy	100%

Table 10: Classification Performance Metrics of the Logistic Regression Model

Risk Category	Precision	Recall	F1-Score	Support
Low	1.00	1.00	1.00	13
Moderate	1.00	1.00	1.00	6
Accuracy			1.00	19
Macro Avg	1.00	1.00	1.00	19
Weighted Avg	1.00	1.00	1.00	19

The results indicate that the model has achieved a 100% level of accuracy, precision, recall, and F1-score. The reason for this is that there is a clear separability of the risk groups. In particular, it is clear that the low-risk group and the moderate-risk group are linearly separable with respect to the concentrations of the radionuclides and the calculated dose indices. Such results have also been obtained in probabilistic risk assessment studies where Monte Carlo simulations have been used to confirm deterministic classifications and the stability of the boundaries in the risk groups under different assumptions on exposure [2].

Similar discriminative power has been observed for the recent applications of logistic regression for radiological risk stratification. In dermatologic radiology, binary logistic regression for distinguishing malignant and benign lesions has been observed to reach perfect classification (AUC = 1.00) when the classes are easily separable [34]. This research is a continuation of these successes of methodology and applies it for dietary radiological risk assessment, validating its use for binary classification when risk classes are easily defined based on radionuclide concentration.

Figure 6 illustrates the confusion matrix for the logistic regression model, where perfect accuracy is observed for distinguishing between low and moderate risk samples. In total, there are 13 true negatives for low-risk samples and 6 true positives for moderate-risk samples, with no false positives and false negatives anywhere. This perfect accuracy suggests a clear distinction exists between different radiological risk classes based on radionuclide concentration. In other research on food safety, confusion matrices are employed for measuring the performance of machine learning algorithms. For instance, 94% accuracy was observed for XGBoost for classifying food ingredients [35], and 93.8% positive predictive accuracy was observed for predicting safety risks [36].

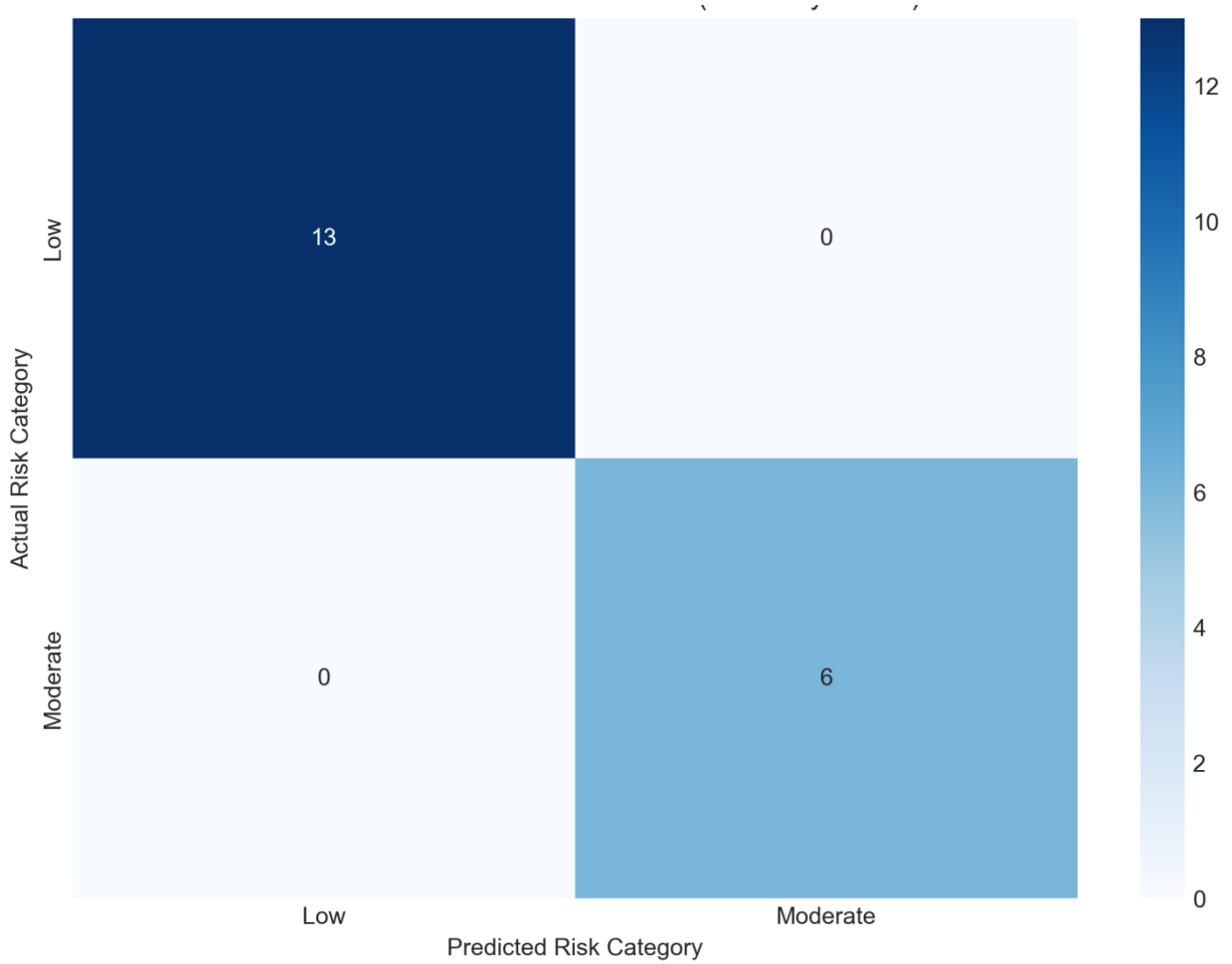

Figure 9: Confusion Matrix for the Logistic Regression Model

The logistic regression probability curve for radiological risk classification is depicted in Figure 10. The curve is characterized by a steep sigmoidal shape that facilitates definitive classification between different risk groups. The curve suggests that it is possible for a clean classification between different risk groups such that samples are classified as either low risk (probability of 0) or moderate risk (probability of 1) without much overlap between classes in the intermediate

region of $0.3 < P < 0.7$. This is indicative of binary separability of the data and is different from the smooth sigmoidal shapes observed in regular logistic regression applications. The risk classification based on radionuclides is highly deterministic in nature.

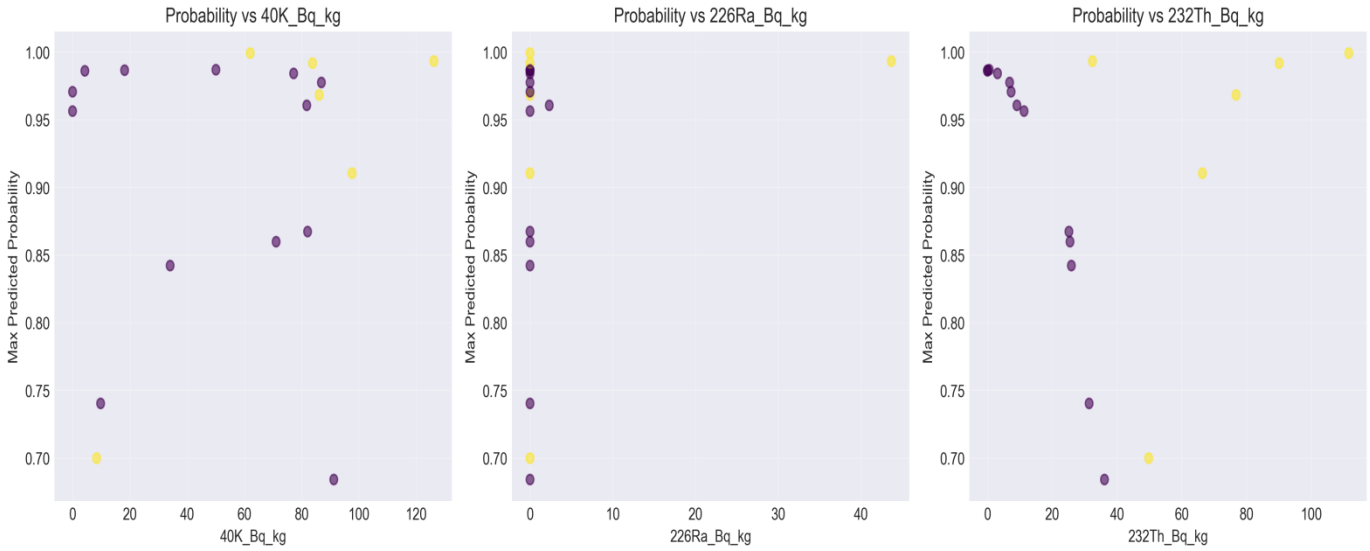

Figure 10: Predicted Probability Distributions by Radionuclide

3.6 Regional Comparison of Radiological Parameters

Mean radionuclide concentrations and associated radiological indices by source region are presented in Table 11.

Table 11: Regional Comparison of Radionuclide Activity Concentrations and Radiological Risk Indices

Region	^{40}K (Bq/kg)	^{226}Ra (Bq/kg)	^{232}Th (Bq/kg)	ACED (µSv/y)	ELCR ($\times 10^{-5}$)
Delta	83.37	2.23	38.80	10.19	2.86
Imported	68.92	0.97	27.76	6.87	1.93
Ogun	105.22	5.61	33.04	9.82	2.75

Spices from Ogun State exhibited higher mean ^{40}K and ^{226}Ra concentrations, while Delta State samples showed elevated ^{232}Th levels. Imported spices consistently recorded lower values, reflecting differences in soil geochemistry and agricultural practices.

A comparison of the regions shows that the concentrations of radionuclides and their dose indices are generally higher in the locally produced spices than in the imported ones. This is expected based on the differences in soil type, use of fertilizers, and climate. Monte Carlo simulations carried out in similar regions have shown similar trends. These have therefore confirmed the influence of geochemical factors in regions on radiological hazards [2].

3.7 Ten-Year Projection of Radiological Exposure

Projected long-term exposure scenarios are summarized in Table 12.

Table 12: Ten-Year Projected Radiological Exposure Under Different Consumption Scenarios

Scenario	^{40}K in 2033 (Bq/kg)	ACED in 2033 (µSv/y)	Total Growth (%)	Description
Conservative	75.38	7.68	+9.61%	Low growth (1% annually)
Moderate	82.37	8.41	+20.02 %	Baseline growth (2% annually)
Aggressive	89.93	9.20	+31.27 %	High growth (3% annually)

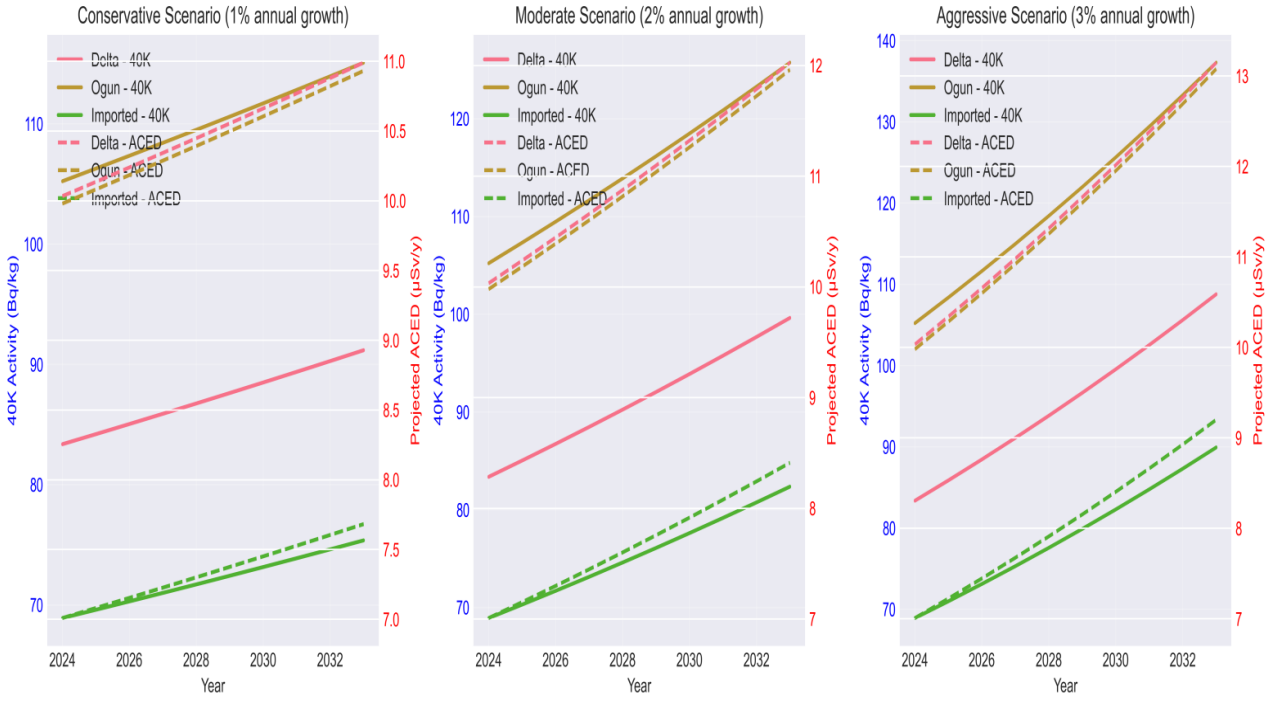

Figure 11: Ten-year Projection of Radiological Exposure under Different Consumption Scenarios

Figure 11 presents a ten years projection of the radiological exposure based on different patterns of consumption. It can be observed that the trends increase linearly while remaining considerably lower than the safety limits. It can be seen that the increase in ^{40}K activity concentration and the corresponding ACED values from 2023 to 2033, based on different rates of increase, is presented in the figure. It can be observed that even in the more aggressive scenario of annual increase of about 3%, the increase in ACED is considerably lower than the ICRP limit of 1 mSv per year on the annual dose to the public [24]. Recent studies based on the Iranian scenario on pasta and other products have shown that even the rare instances with higher ^{232}Th concentrations, up to 45.72 µSv per year, are only 0.02% of the ICRP annual limit and thus do not pose a radiological health hazard due to the presence of natural radioactivity in the diet [37]. It can thus be clearly deduced that there is no radiological hazard in consuming these spices.

Figure 12 shows a Monte Carlo projection that illustrates the distribution of dose estimates, with 95% confidence limits to indicate the probable range in which the real values exist. These shaded areas indicate the degree of uncertainty in the calculated mean predictions, and even with the inclusion of different rates of intake and different levels of radionuclides, the upper end does not approach the limits set by the authorities. This probabilistic validation of the deterministic calculations further confirms the long-term risk assessment and supports the claim that there is no radiological health hazard in the consumption of spice.

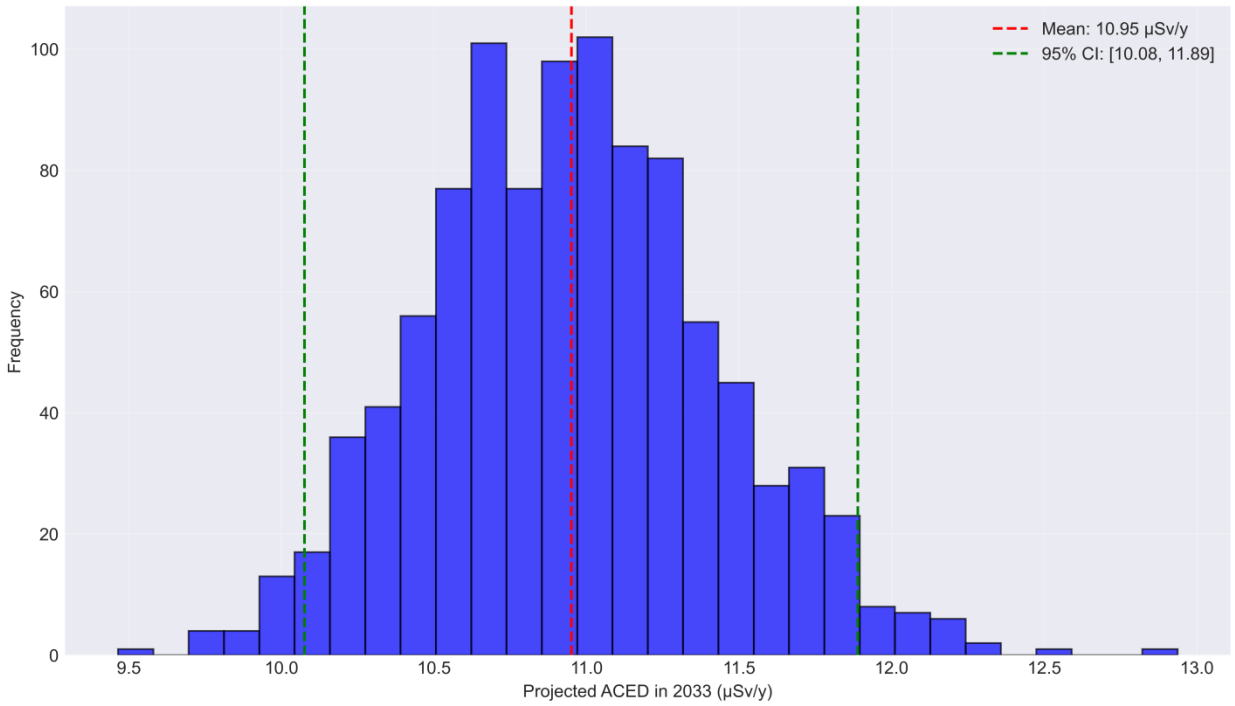

Figure 12: Monte Carlo Simulation of the Projected Annual Dose Distribution

4. CONCLUSION

The research provides an extensive assessment of long-term exposure to radiation that occurs with the use of common spices consumed in Southern Nigeria by combining measured activity concentrations with deterministic and predictive statistical models. The results reveal that naturally occurring radioisotopes (^{40}K, ^{226}Ra, and ^{232}Th) are distributed at different levels in both locally and foreign spices, with ^{40}K having the highest mean activity concentration because of its ubiquitous nature, and ^{232}Th being identified as the major contributor to ingestion hazards.

Notwithstanding the variations that can be related to the type of spice, soil geochemistry, and agricultural practices, the annual committed effective doses (ACED) and excess lifetime cancer risks (ELCR) for all samples are well below the recommended internationally accepted safety standards. The correlations between ^{232}Th and ACED and between ^{232}Th and ELCR are strong, thus establishing that the key factor in determining the doses is indeed ^{232}Th, as indicated by established dose conversion factors. The validity of the multiple linear regression model also verifies that the ingestion dose is a deterministic process that can be predicted by activity concentrations of the radionuclides.

The results of multi-variate analysis and principal component analysis show specific accumulation patterns for potassium/thorium series and radium series radionuclides. In fact, the results of logistic regression analysis show accurate classification of spice samples into low and moderate risk groups. The results thus indicate clearly defined boundaries of radiological risk. The results of this deterministic analysis are consistent with previous probabilistic results of Monte Carlo analysis done in a similar setting in Nigeria.

Even in aggressive growth rates of consumption, long-term predictions forecast that cumulative doses are still well below the public dose limit of 1 mSv/y recommended by international radiological protection organizations. Therefore, it can be concluded that there are no significant radiological health concerns associated with the normal consumption of these analyzed spice samples. Notably, this research work contributes to the current body of knowledge by not only conducting an assessment of exposure to radionuclides through food consumption but also by developing a predictive model for long-term dietary exposure to radionuclides. The framework proposed in this paper can be applied to monitoring, making health-related decisions, and further studies to enhance models for other food groups to better understand their dietary exposure. Ongoing monitoring is also advised to reflect any possible shifts in agricultural and consumption trends.

5. REFERENCES

[1] Kolapo, A. A., & Omoboyede, J. O. 2018. Health risk assessment of natural radionuclide and heavy metals in commonly consumed medicinal plants in south-west Nigeria. Ife Journal of Science, 20(3), 529-537.

[2] Okeyode, I. C., Amuofu, J. A., Isinkaye, M. O., Mustapha, A. O., Oluwalana, S. A., & Ewumi, T. O. 2025. Monte Carlo simulations of radiological cancer risks associated with naturally occurring radionuclides in local and imported spices from Delta and Ogun States, Nigeria. International Journal of Environmental Health Research, 35(9), 2277-2288.

[3] Gupta, D. K., Chatterjee, S., Datta, S., Voronina, A. V., & Walther, C. 2016. Radionuclides: accumulation and transport in plants. Rev Environ Contam Toxicol, 241, 139-160.

[4] Tiwari, S. N., Raj, S. S., Kumar, D., & Gocher, A. K. 2024. Assessment of Radionuclide Transfer in Terrestrial Ecosystem. In Handbook on Radiation Environment, Volume 1: Sources, Applications and Policies (pp. 121-159). Singapore: Springer Nature Singapore.

[5] Olusola, J. A., Akintan, O. B., & Osanyinlusi, O. 2025. Trace metals potential human health risks assessment through consuming common food spices in Ado Ekiti, Southwest,

Nigeria. Journal of Trace Elements and Minerals, 11, 100208.

[6] López-Romero, J. C., González-Ríos, H., Peña-Ramos, A., Velazquez, C., Navarro, M., Robles-Zepeda, R., & Hernández, J. 2018. Seasonal effect on the biological activities of Litsea glaucescens Kunth extracts. Evidence-Based Complementary and Alternative Medicine, 2018(1), 2738489.

[7] Ivanišová, E. 2023. Herbs and Spices: New Advances, Intech Open, pp. 1-280.

[8] Olaiwola, M. A., Olubunmi, O. M., Owolabi, S. A., Senami, A., & Oluwafunmilola, M. H. O. 2025. Assessment of Trace Metals Load and Potential Health Risks Associated with Some Common Tropical Plant Spices in Nigeria. SSRG International Journal of Agriculture & Environmental Science, 12(2), 1-10.

[9] Akinola, R., Pereira, L. M., Mabhaudhi, T., De Bruin, F. M., & Rusch, L. 2020. A review of indigenous food crops in Africa and the implications for more sustainable and healthy food systems. Sustainability, 12(8), 3493.

[10] Ononugbo, C. P., Avwiri, G. O., & Ikhuiwu, S. O. 2017. Estimation of natural radioactivity levels in some food spices commonly used in Nigeria and its radiological risks. Journal of Scientific Research and Reports, 16(3), 1-9.

[11] Ugbede, F. O., Agbajor, G. K., Akpolile, A. F., Popoola, F. A., Okoye, O. N., Akpobasahan, E. A., & Umeche, M. A. 2023. Ingestion exposure of public to natural radionuclides and committed effective dose and cancer risk through tuber crops cultivated in Ebonyi State, Nigeria. Environmental Monitoring and Assessment, 195(11), 1385.

[12] United Nations Scientific Committee on the Effects of Atomic Radiation. 2008. Sources and effects of ionizing radiation (Annex B). UNSCEAR.

[13] International Atomic Energy Agency (IAEA). 2023. Exposure due to radionuclides in food other than during a nuclear or radiological emergency: Technical material (Safety Reports Series No. 114). IAEA.

[14] Lenka, P., Sahoo, S. K., Mohapatra, S., Patra, A. C., Dubey, J. S., Vidyasagar, D., & Puranik, V. D. 2013. Ingestion dose from 238U, 232Th, 226Ra, 40K and 137Cs in cereals, pulses and drinking water to adult population in a high background radiation area, Odisha, India. Radiation protection dosimetry, 153(3), 328-333.

[15] Wais, T. Y., Namq, B. F., Najam, L. A., Živković, M. P., Najemalden, M. A., Ahmed, R. T., ... & Mansour, H. 2025a. Assessment of natural radioactivity and dietary exposure to 238U, 232Th, and 40K in commonly consumed foods from Kirkuk Governorate, Iraq. Journal of Food Composition and Analysis, 108431.

[16] Hastie, T., Tibshirani, R., & Wainwright, M. 2015. Statistical learning with sparsity. Monographs on statistics and applied probability, 143(143), 8.

[17] Naji, M. A., El Filali, S., Aarika, K., Benlahmar, E. H., Abdelouhahid, R. A., & Debauche, O. 2021. Machine learning algorithms for breast cancer prediction and diagnosis. Procedia Computer Science, 191, 487-492.

[18] Greenacre, M., Groenen, P. J., Hastie, T., d'Enza, A. I., Markos, A., & Tuzhilina, E. 2022. Principal component analysis. Nature Reviews Methods Primers, 2(1), 100.

[19] Abdi, H., & Williams, L. J. 2010. Principal component analysis. Wiley interdisciplinary reviews: computational statistics, 2(4), 433-459.

[20] Sivapriya, J., Kumar, A., Sai, S. S., & Sriram, S. 2019. Breast cancer prediction using machine learning. International Journal of Recent Technology and Engineering (IJRTE), 8(4), 4879-4881.

[21] Omoriwhovo, J.O., Agbajor, G.K., Akpolilie, A.L. and Akpojotor, G. 2022. Python AIM Solver to Obtain the Vibrational Energy Spectra of Diatomic Molecules. African Journal of Physics, 15:15-31.

[22] Saleh, D. S., Salh, H., Smail, J. M., Ahmad, S. T., & Kareem, S. R. 2024. Estimation of radiological health risks due to 226Ra, 232Th, and 40K in foods consumed in Iraqi Kurdistan Region. Isotopes in Environmental and Health Studies, 60(6), 628-641.

[23] Wais, T. Y., Namq, B. F., Najam, L. A., Othman, S. Q., Hussein, Z. A., Al-Taii, H. A., ... & Kumar, A. 2025b. Investigation of natural radionuclide transfer from soil to wheat. Scientific Reports, 15(1), 35785.

[24] International Atomic Energy Agency (IAEA). 2019. Radionuclides in Food and Drinking Water in Non-Emergency Situations. Joint EPReSC8-RASSC46 Session.

[25] Gomes, P. D. S., de Barcelos, A. A., Cabral, J. B. P., Ramalho, F. L., Rocha, H. M., Becegato, V. A., & Paulino, A. T. 2026. Content of Radionuclides in Soils of Hydraulic Development Areas in Brazil. Soil Systems, 10(1), 10.

[26] Yarima, M. H., Khandaker, M. U., Nadhiya, A., & Olatunji, M. A. 2019. Assessment of natural radioactivity in maize and estimation of concomitant dose to Nigerian via ingestion pathway. Radiation Protection Dosimetry, 184(3-4), 359-362.

[27] Expósito-Suárez, V. M., Suárez-Navarro, J. A., Morales-Quijano, M., Gómez-Mancebo, M. B., Barragan, M., Cortecero, M., & Benavente, J. F. 2024. Modelling the Uptake of 226Ra and 238U Stable Elements in Plants during Summer in the Vicinity of Tailings from an Abandoned Copper Mine. Applied Sciences, 14(20), 9201.

[28] Wais, T. Y., Namq, B. F., Najam, L. A., Othman, S. Q., Hussein, Z. A., Al-Taii, H. A., ... & Kumar, A. 2025b. Investigation of natural radionuclide transfer from soil to wheat. Scientific Reports, 15(1), 35785.

[29] Mwimanzi, J. M., Haneklaus, N. H., Lolila, F., Marwa, J. J., Rwiza, M. J., & Mtei, K. M. 2025. Age-Stratified spatial radiological risk assessment of 226Ra 232Th and 40K in water surrounding the Geita gold mine in Tanzania. Journal of Xenobiotics, 15(5), 152.

[30] Rao, S., Sharan, K., Chandraguthi, S. G., Dsouza, R. N., David, L. R., Ravichandran, S., ... & Ozsahin, D. U. 2024. Advanced computational methods for radiation dose optimization in CT. Diagnostics, 14(9), 921.

[31] Wang, P., Huang, W., Zou, H., Lou, X., Ren, H., Yu, S., ... & Cao, Y. 2024. Model prediction of radioactivity levels in the environment and food around the world's first AP 1000 nuclear power unit. Frontiers in Public Health, 12, 1400680.

[32] Baez, G. R., García, H., Grosenick, D., & Wabnitz, H. 2019. Implementation of the extended Kalman filter for determining the optical and geometrical properties of

turbid layered media by time-resolved single distance measurements. Biomedical Optics Express, 11(1), 251-266.

[33] Shpigelman, E., & Shamir, R. 2023. A feature ranking algorithm for clustering medical data. medRxiv, 2023-09.

[34] Tiryaki Baştuğ, B., Gencer Başol, H., Dursun Çoban, B., Topuz, S., & Türelik, Ö. 2025. A Novel Radiology-Adapted Logistic Model for Non-Invasive Risk Stratification of Pigmented Superficial Skin Lesions: A Methodological Pilot Study. Diagnostics, 15(15), 1921.

[35] Rai, B. K., Chandan, N. S., Marangappanavar, D. N., Indira, S., & Kumar, G. 2025. Classifying food ingredients using machine learning on nutritional and biochemical data. Discover Food, 5(1), 382.

[36] Wu, D., Cai, H., & Li, T. 2025. Food Safety Risk Prediction and Regulatory Policy Enlightenment Based on Machine Learning. Systems, 13(8), 715.

[37] Sadeghi, H., Pourimani, R., & Feyzi, M. 2025. Radiological assessment and dose evaluation from natural radionuclides in common pasta. Scientific Reports, 15(1), 44187.